Oscillations of relativistic axisymmetric tori and implications for modelling kHz-QPOs in neutron-star X-ray binaries

P. J. Montero[1][*], O. Zanotti[2]

[1]*Max-Planck-Institut für Astrophysik, Karl-Schwarzschild-Strasse 1, D-85748, Garching bei Mnchen, Germany*
[2]*Max-Planck-Institut für Gravitationsphysik, Albert Einstein Institut, Am Mühlenberg 1, 14476, Golm, Germany*

ABSTRACT

We perform a global linear perturbative analysis, and investigate the oscillation properties of relativistic, non-selfgravitating tori orbiting around neutron stars in the slow rotation limit approximation. Extending the work done in Schwarzschild and Kerr backgrounds, we consider the axisymmetric oscillations of vertically integrated tori in the Hartle-Thorne spacetime. The equilibrium models are constructed by selecting a number of different non-Keplerian distributions of specific angular momentum, allowing for disc sizes $L \sim 0.5 - 600$ gravitational radii. Our results, obtained after solving a global eigenvalue problem to compute the axisymmetric p-modes, indicate that such oscillation modes could account with most observed lower (ν_L) and upper (ν_U) high frequency quasi-periodic oscillations for Sco X-1, and for some Z sources and Atoll sources with $\nu_L \gtrsim 500$ Hz. However, when $\nu_L \lesssim 500$ Hz, p-modes oscillations do not account for the linear relation $\nu_U = A\nu_L + B$, $B \neq 0$ between the upper and the lower high frequency quasi-periodic oscillations that are observed in neutron star low-mass X-ray binaries.

Key words: X-rays: binaries – relativity – stars: neutron

1 INTRODUCTION

Quasi-periodic oscillations (QPOs) observed in the X-ray spectra of binary systems are transient phenomena associated to non-thermal states and state transitions. Those observed at high frequencies, in the range $\sim 200 - 1200$ Hz (van der Klis 2005), are referred to as high frequency QPOs (kHz-QPOs). An important feature of such kHz-QPOs is that they usually appear in couples consisting of a lower and an upper kHz-QPO. The entire set of kHz-QPOs detected in black hole binaries (BHBs), i.e. binaries having a black hole as an accretor, contains only seven sources[1], four of which[2] show both the upper and the lower kHz-QPO. On the other hand, there are approximately 20 neutron stars binaries (NSBs), i.e. binaries having a neutron star as the accretor, that show the kHz-QPO phenomenology (see Miller (2010) for a recent review about QPOs in NSBs), including both Z and Atoll type (Lewin & van der Klis 2006). Interestingly, these QPO frequencies correspond to the frequencies of orbits a few gravitational radii away from a stellar-mass compact object, which explains why kHz-QPOs have been considered a promising tool to investigate the gravitational forces in the strong field regime. It should also be noted, however, that in a recent work Sanna et al. (2010) have shown that the NSB J1701-462 provides an example of a source that, during the same outburst, presents

spectral and timing characteristic of both Z and Atoll sources. Because the kHz-QPOs detected are remarkably different in the two spectral states, and because such differences cannot be attributed to changes in the gravitational field of the central compact object, the authors conclude that the coherence and rms amplitude of the kHz-QPOs cannot be used to deduce the existence of the innermost stable circular orbit around a neutron star.

Although it is still not clear whether there is a unique physical mechanism responsible for the generation of kHz-QPOs in both BHBs and NSBs, a few observational evidences have emerged over the years which may indicate the existence of *two distinct* mechanisms.

• First of all, the kHz-QPO peak separation in NSBs is typically within 20% of the neutron star spin frequency $\nu_{\rm spin}$, or half of that (van der Klis 2005). In particular, sources with $\nu_{\rm spin} < 400 Hz$ always have $\Delta\nu \sim \nu_{\rm spin}$, while sources with $\nu_{\rm spin} > 400 Hz$ always have $\Delta\nu \sim \nu_{\rm spin}/2$ (Muno et al. 2001).

• Secondly, while in NSBs the frequencies observed may vary by a factor 2 in association to changes of the luminosity, the frequencies in BHBs are much more stable and vary at most by 15%, even when the luminosity changes by a factor 3 (Remillard & McClintock 2006). This effect is clearly shown in Fig. 1 by Belloni et al. (2005) or in Fig. 3 by Török et al. (2006), where the upper frequencies, ν_U, are plotted versus the lower frequencies, ν_L; showing that while kHz-QPOs from a *single* BHB are represented essentially as a point, kHz-QPOs from a

---

[1] See Remillard & McClintock (2006) for a review on X-ray properties of BHBs.
[2] GRS 1915+105, GRO 1655-40, XTE J1550-564 and H 1743-322.

single NSB are scattered along straight lines, the so called "Bursa lines" (Abramowicz et al. 2007; Török et al. 2006).

• An additional peculiar property of twin kHz-QPOs in the four BHBs where they have been simultaneously observed is that such frequencies appear in couples obeying the ratio $3 : 2$ to a high degree of accuracy (see Fig.1 by Török et al. (2005)). Over the last few years there has been an ongoing debate about the existence of the same phenomenology among kHz-QPOs in NSBs. Observations, in fact, clearly indicate that Bursa lines $\nu_U = A\nu_L + B$ of kHz-QPOs in NSBs are not compatible with a constant $3 : 2$ ratio ($A = 1.5$, $B = 0$), but it remains controversial whether the peak at 1.5 in the distribution of the observed ν_U/ν_L ratios is physical or not (Belloni et al. 2005; Török et al. 2006; Belloni et al. 2007; Török et al. 2008; Boutelier et al. 2010).

Several models have been proposed over the years to explain the physical mechanism responsible for the generation of kHz-QPOs in the X-ray spectra of binary systems (Miller et al. 1998; Stella & Vietri 1999; Lamb & Miller 2003; Abramowicz et al. 2003; Rezzolla et al. 2003; Zhang 2004; Arras et al. 2006). In particular, the model proposed by Rezzolla et al. (2003) for kHz-QPOs in BHBs suggests the existence of an oscillating torus around the black hole, and identifies the time variability in the X-ray spectra with inertial-acoustic modes (p-modes) of the relativistic thick accretion torus which acts as a resonant cavity for the p-mode axisymmetric oscillations. The frequencies of the fundamental and the first-overtone modes appear approximately in a $3 : 2$ ratio, and within the range of kHz-QPOs depending on the spin of the black hole and the size of the torus. Moreover, the model by Rezzolla et al. (2003) also accounts for the M^{-1} scaling of the frequency, where M is the mass of the black hole.

The main properties of the axisymmetric p-mode oscillations of relativistic, non-selfgravitating tori orbiting black holes have been investigated in a series of papers either using a linear perturbative approach by Rezzolla et al. (2003); Montero et al. (2004) (hereafter Paper I and Paper II, respectively) or through non-linear general relativistic hydrodynamic simulations of both, non-selfgravitating tori (Zanotti et al. 2003; Zanotti et al. 2005; Montero et al. 2007) and also selfgravitating tori (Montero et al. 2008, 2010). The linear perturbative approach, computationally less demanding, allows for a more detailed investigation of the parameter space. Overall, those perturbative analysis confirmed the results of non-linear hydrodynamic simulations which revealed that the lowest-order eigenfrequencies appear in a sequence of small integers 2:3:4..., for a wide range of models. It is also worth noting that some of these modes have been related in the analysis performed by Blaes et al. (2006) to surface gravity waves, at least in the slender torus limit.

However, it remains unclear whether a kHz-QPO model based on axisymmetric inertial-acoustic oscillations is flexible enough to explain the rich phenomenology of kHz-QPOs in NSBs, and in particular to account for the distribution of the upper and the lower kHz-QPOs along the "Bursa lines" observed in NSBs. To address this question we perform a global linear perturbative analysis of equilibrium thick discs around neutron stars, whose external metric is described in the slow limit approximation. The set of perturbed relativistic equations is reduced to the solution of an eigenvalue problem, following the approach described in Paper I and II. In order to explore exhaustively the deviations from the $3 : 2$ ratio that axisymmetric inertial-acoustic oscillations display, we consider a much wider parameter space than that studied in Paper I and II,

particularly in terms of the rotation law and the extension of the accretion disc.

The plan of the paper is as follows: in Section 2 we introduce the basic assumptions and equations employed in the definition of our general relativistic, vertically integrated tori. In Section 3 we derive the perturbation equations, and in Section 4 we list the properties of the non-selfgravitating equilibrium models studied. In Section 5, on the other hand, we present the results of the global analysis, while Section 6 is devoted to a discussion of the implications for explaining kHz-QPOs in NSBs. Finally, Section 7 contains our conclusions.

In the following we will assume a signature $\{-, +, +, +\}$ for the space-time metric and we will use Greek letters $\mu, \nu, \lambda, \ldots$ (running from 0 to 3) for four-dimensional space-time tensor components, while Latin letters $i, j, k, \ldots$ (running from 1 to 3) will be employed for three-dimensional spatial tensor components. We also adopt a geometrized system of units by setting $c = G = 1$.

2   EQUILIBRIUM TORI IN THE HARTLE-THORNE SPACETIME

Equilibrium thick discs around a rotating neutron star are constructed assuming that their self-gravity can be neglected and that the background spacetime takes the form of the Hartle-Thorne metric (Hartle & Thorne 1968), which describes the metric around a slowly rotating neutron star. Since we are interested in the region of the spacetime around the equatorial plane, we use cylindrical coordinates (t, ϖ, ϕ, z), and consider only the zeroth-order terms in the ratio z/ϖ (Wilson 1972; Novikov & Thorne 1973), where ϖ is the cylindrical radial coordinate (see Eq. (1) in Paper II for this form of the Kerr line element). Then the Hartle-Thorne metric in cylindrical coordinates derives from the Kerr metric, in Boyer-Lindquist coordinates, by retaining only those terms which are first order in the ratio a/ϖ, where a is the Kerr parameter, and by replacing the spin of the black hole with the angular momentum of the neutron star. In this way we obtain

$$\Delta = \varpi^2 - 2M\varpi + a^2 = \varpi^2(1 - \frac{2M}{\varpi} + \frac{a^2}{\varpi^2})$$
$$\simeq \varpi^2(1 - \frac{2M}{\varpi}) \,, \tag{1}$$

$$A = \varpi^4 + \varpi^2 a^2 + 2M\varpi a^2 = \varpi^4(1 + \frac{a^2}{\varpi^2} + 2\frac{M}{\varpi}\frac{a^2}{\varpi^2})$$
$$\simeq \varpi^4 \,, \tag{2}$$

$$\omega = \frac{2Ma\varpi}{A} \simeq \frac{2J}{\varpi^3} \,, \tag{3}$$

where M is the neutron star mass, and J is the angular momentum of the neutron star (Rezzolla et al. 2001), which we assume to be constant. Then the line element of the Hartle-Thorne metric becomes

$$ds^2 = -\left(1 - \frac{2M}{\varpi}\right) dt^2 + \left(1 - \frac{2M}{\varpi}\right)^{-1} d\varpi^2$$
$$-2\omega\varpi^2 d\phi dt + \varpi^2 d\phi^2 + dz^2 \,. \tag{4}$$

In order to construct hydrostatic equilibrium models of rotating thick discs we solve the continuity equation $\nabla_\alpha(\rho u^\alpha) = 0$ and the conservation of energy-momentum, $\nabla_\alpha T^{\alpha\beta} = 0$, where the symbol ∇ refers to a covariant derivative with respect to the metric (4). Here, $T^{\alpha\beta} \equiv (e + p)u^\alpha u^\beta + pg^{\alpha\beta}$ are the components of the stress-energy tensor of a perfect fluid, with u^α being the compo-

nents of the 4-velocity, ρ the rest-mass density, e the energy density and p the pressure.

It is also useful to introduce an orthonormal tetrad carried by the local stationary observer and defined by the one-forms with components

$$\boldsymbol{\omega}^{\hat{t}} = \varpi\sqrt{\Delta/A}\mathbf{d}t , \qquad \boldsymbol{\omega}^{\hat{\phi}} = \sqrt{A}(\mathbf{d}\phi - \omega\mathbf{d}t)/\varpi ,$$
$$\boldsymbol{\omega}^{\hat{z}} = \mathbf{d}z , \qquad \boldsymbol{\omega}^{\hat{\varpi}} = \varpi/\sqrt{\Delta}\mathbf{d}\varpi . \tag{5}$$

In this frame, the components of the four velocity of the fluid are denoted by $u^{\hat{\mu}}$ and the 3-velocity components are defined as

$$v^{\hat{i}} \equiv \frac{u^{\hat{i}}}{u^{\hat{t}}} = \frac{\omega_\alpha^{\hat{i}} u^\alpha}{\omega_\alpha^{\hat{t}} u^\alpha} , \qquad i = \varpi, z, \phi . \tag{6}$$

We consider a perfect fluid that follows a polytropic equation of state (EOS) $p = k\rho^\gamma$, where k and $\gamma \equiv d\ln p/d\ln\rho$ are the polytropic constant and the adiabatic index, respectively. Next, following Paper I & II, we introduce a vertically integrated pressure

$$P(\varpi) \equiv \int_{-H}^{H} p\,dz, \tag{7}$$

and a vertically integrated rest-mass density

$$\Sigma(\varpi) \equiv \int_{-H}^{H} \rho\,dz, \tag{8}$$

where $H = H(\varpi)$ is the local "thickness" of the torus. We further assume that P and Σ obey an "effective" polytropic EOS

$$P = \mathcal{K}\Sigma^\Gamma , \tag{9}$$

so that $\mathcal{K}$ and $\Gamma \equiv d\ln P/d\ln\Sigma$ play the role of the polytropic constant and of the adiabatic index, respectively.

After the vertical integration, we enforce the conditions of hydrostatic equilibrium and axisymmetry (*i.e.* assume $\partial_t = 0 = \partial_\phi$) and simplify the equation of energy-momentum conservation to a Bernoulli-type form (Kozlowski et al. 1978)

$$\frac{\partial_i P}{E + P} = -\left(\partial_i \ln u^t - \frac{\ell}{1 - \Omega\ell}\partial_i\Omega\right) , \tag{10}$$

where $\ell \equiv -u_\phi/u_t$ is the specific angular momentum, $\Omega = u^\phi/u^t$ is the angular velocity and

$$(u^t)^{-2} = -(g_{tt} + 2\Omega g_{t\phi} + \Omega^2 g_{\phi\phi}) . \tag{11}$$

After simple manipulations Eq. (10) can be rewritten as

$$\partial_i \ln u^t - \frac{\ell}{1 - \Omega\ell}\partial_i\Omega = \frac{(u^t)^2}{2}\left(\partial_i g_{tt} + 2\Omega\partial_i g_{t\phi} + \Omega^2\partial_i g_{\phi\phi}\right) . \tag{12}$$

By using the metric terms of (4) into (10), we derive the following force balance equation for a non-selfgravitating disc in the Hartle-Thorne spacetime

$$\frac{1}{E + P}\frac{dP}{d\varpi} = -\frac{M/\varpi^2 - \Omega\varpi(\omega + \Omega)}{\left(1 - \frac{2M}{\varpi}\right) + \Omega\varpi^2(2\omega - \Omega)}, \tag{13}$$

where E is the vertically integrated energy density, defined in complete analogy to (7) and (8).

3 PERTURBATION EQUATIONS

We next perturb the hydrodynamical equations introducing Eulerian perturbations of the hydrodynamical variables with a harmonic time dependence of the type

$$\left(\delta V^{\hat{\varpi}}, \delta V^{\hat{\phi}}, \delta Q\right) \sim \exp(-i\sigma t) , \tag{14}$$

Table 1. Main properties of the equilibrium models studied. From left to right the columns report: the name of the model, the type of specific angular momentum distribution, the constant coefficient ℓ_c, the power-law index q (*cf.* eq. 21) or its range of values, the minimum radial size for the corresponding sequence of tori, and the maximum radial size for the sequence of tori. The angular momentum of the neutron star is set to be $J = 0.1$ in all of the models.

Model	$\ell(\varpi)$	ℓ_c	q	L_{min}	L_{max}
A1	const.	3.60	0.0	0.4	1.9
A2	const.	3.65	0.0	0.5	5.7
A3	const.	3.70	0.0	0.5	10.0
A4	const.	3.75	0.0	0.4	16.8
A5	const.	3.80	0.0	0.8	29.9
A6	const.	3.85	0.0	0.7	71.4
B1	power-law	3.0	[0.1, 0.15]	2.5	374.3
B2	power-law	3.1	[0.08, 0.15]	2.1	348.6
B3	power-law	3.2	[0.07, 0.15]	1.9	279.6
B4	power-law	3.3	[0.05, 0.15]	0.8	318.4
B5	power-law	3.4	[0.04, 0.15]	2.5	363.3
B6	power-law	3.5	[0.02, 0.15]	1.7	265.3
B7	power-law	3.6	[0.006, 0.15]	0.4	327.1
B8	power-law	3.7	[0.001, 0.15]	1.9	276.7
B9	power-law	3.8	[0.001, 0.15]	2.6	299.1
B10	power-law	3.9	[0.001, 0.15]	2.7	281.6
C1	power-law	2.59	0.2	3.3	160.8
C2	power-law	2.15	0.3	5.3	548.8
C4	power-law	2.19	0.3	7.6	575.1
C5	power-law	2.29	0.3	1.4	550.9
C6	power-law	2.35	0.3	1.9	545.1
C7	power-law	2.39	0.3	0.7	156.6
C8	power-law	1.79	0.4	51.5	593.9

where $\delta Q \equiv \delta P/(E+P)$ and where we have defined the vertically averaged velocity perturbations respectively as

$$\delta V^{\hat{\varpi}} \equiv \frac{1}{2H}\int_{-H}^{H}\delta v^{\hat{\varpi}}dz , \qquad \delta V^{\hat{\phi}} \equiv \frac{1}{2H}\int_{-H}^{H}\delta v^{\hat{\phi}}dz . \tag{15}$$

We assume that the Eulerian perturbations in the metric functions can be neglected, *i.e.* $\delta g_{ab} = 0$ (Cowling approximation; Cowling, 1941). While this condition does not hold in general, it represents a very good approximation in the case of non-selfgravitating tori.

To eliminate the imaginary part from the system of equations we introduce the following quantities

$$\delta U \equiv i\delta V^{\hat{\varpi}} , \qquad \delta W \equiv \delta V^{\hat{\phi}} , \tag{16}$$

and after a bit of straightforward algebra, we derive the following set of ordinary differential equations

$$\sigma\frac{\Delta}{\sqrt{A}}\delta U + \alpha\frac{\Delta}{\varpi^2}\delta Q' + \left[\frac{\Delta^{3/2}}{A}\left(\frac{A}{\varpi^2}\right)'\Omega - \frac{\Delta^{3/2}}{A}\left(\frac{A\omega}{\varpi^2}\right)' + 2\frac{\Delta^{3/2}}{\varpi^2}(\Omega - \omega)\frac{P'}{E+P}\right]\delta W = 0 , \tag{17}$$

$$\sigma \frac{\varpi^2 \sqrt{\Delta}}{A} \delta W + \left\{ \Omega' + \Omega \ln \left(\frac{A}{\varpi^2} \right)' + \right.$$

$$\frac{A}{\varpi^2 \Delta} \left(\frac{\varpi^2 \Delta}{A} \right)' (\omega - \Omega) -$$

$$\left. \frac{A^2 \omega'}{\varpi^4 \Delta} \Omega^2 - \frac{\varpi^2}{A} \left(\frac{A\omega}{\varpi^2} \right)' \right\} \frac{\Delta}{\sqrt{A}} \delta U + \frac{A \sigma \alpha}{\Delta \varpi^2} (\omega - \Omega) \delta Q = 0 , \tag{18}$$

$$\sigma \delta Q + \widetilde{\Gamma} \frac{\Delta}{\sqrt{A}} \delta U' + \left\{ \frac{\Delta}{\sqrt{A}} \left[\frac{P'}{E + P} + \right. \right.$$

$$\left. \left. \widetilde{\Gamma} \left(\frac{1}{\varpi} - \frac{1}{2} \ln \left(\frac{r^2 \Delta}{A} + \frac{A}{\varpi^2} \Omega(2\omega - \Omega) \right)' \right) \right] \right\} \delta U$$

$$- \left(\frac{\sigma \sqrt{\Delta}(\omega - \Omega) A \varpi^2}{\varpi^4 \Delta + A^2 \Omega(2\omega - \Omega)} \right) \widetilde{\Gamma} \delta W = 0 , \tag{19}$$

where $\alpha \equiv 1/(u^t)^2$, $\widetilde{\Gamma} \equiv \Gamma P/E + P$, and the index $'$ indicates the derivative with respect to ϖ.

Equations (17)–(19) are the ϖ- and ϕ-components of the perturbed relativistic Euler equations and the perturbed continuity equation, respectively. They can be solved numerically for the eigenfrequencies and for the eigenfunctions of p-mode oscillations of an oscillating vertically integrated thick disc in the Hartle-Thorne spacetime. In practice, we solve the system of equations (17)–(19) as an eigenvalue problem using a "shooting" method (Press et al., 1986) in which, once the appropriate boundary conditions are provided, two trial solutions are found, starting from the inner and outer edges of the disc respectively, and these are then matched at an intermediate point where the Wronskian of the two solutions is evaluated. This procedure is iterated until a zero of the Wronskian is found, thus providing a value for σ and a solution for $\delta Q, \delta U$, and δW. The numerical method employed here to solve the eigenvalue problem is the same as that discussed in Paper I and Paper II, where a more detailed discussion can be found.

4 EQUILIBRIUM MODELS

First of all, we fix the angular momentum of the star which is defined as $J = I\Omega_\star$, where $\Omega_\star = 2\pi/P_\star$ is the angular velocity of the star. In geometrized units we have

$$J = \frac{I_{45}}{P_1} \left(\frac{M_\odot}{M} \right)^2 7.1363 \times 10^{-4} \tag{20}$$

where I_{45} is the moment of inertia of the star in units of 10^{45}g cm^2, which we take as $I_{45} = 1.0$, while P_1 is the period of rotation in units of sec. For instance, the typical Atoll source 4U 1608-52 (van Straaten et al. 2003) has a mass $M = 1.7 M_\odot$, a spin period of $P = 1.61$ms, and the angular momentum, computed from Eq. (20), is therefore $J = 0.15$. Even assuming a binary system with an accreting neutron star that rotates as fast as the fastest known millisecond pulsar PSR J1748-2446ad, namely with P=1.39 msec, and with a canonical mass $M = 1.4 M_\odot$, would yield to $J = 0.26$.

In Sections 5 and 6 below we report results obtained after assuming $J = 0.1$. However, we have also solved the eigenvalue problem for the case $J = 0.2$, without finding any significant difference in the results, so that our conclusions remain unchanged.

Next we define the distribution of the specific angular momentum $\ell = \ell(\varpi)$ within the disc. We consider tori with distributions of specific angular momentum that are constant in space, *i.e.* $\ell(\varpi) = \text{const.}$, and also tori with non-constant distributions of the specific angular momentum[3]. We note that $\ell(\varpi) = \text{const.}$ is a useful mathematical case which leads to analytic initial data, while non-constant distributions of the specific angular momentum are a more realistic assumption. In the case of $\ell(\varpi) = \text{const.}$, the value of the specific angular momentum must satisfy the condition $\ell_{\text{ms}} < \ell < \ell_{\text{mb}}$, where ℓ_{ms} and ℓ_{mb} are the specific angular momenta of the marginally stable and of the marginally bound orbit in the Hartle-Thorne spacetime (see e.g. Abramowicz et al. (2003)). On the other hand, in the case of tori with non-constant distributions of the specific angular momentum, we consider a power-law distribution of the type

$$\ell = \ell_c \varpi^q , \tag{21}$$

where both ℓ_c and q are positive constants. The power-law angular momentum distributions are chosen such that the position of the cusp is always located between the marginally bound and the marginally stable orbits. The position of the cusp, as well as the position of the maximum rest-mass density ϖ_{max} in the torus, are obtained by imposing that the specific angular momentum at these two points coincides with the Keplerian value (Kozlowski et al. 1978). The inner edge of the torus ϖ_{in} is determined by fixing the potential gap $\Delta W_{in} = W_{\text{in}} - W_{\text{cusp}}$, defined as

$$\Delta W_{\text{in}} = \ln[(-u_t)_{\text{in}}] - \ln[(-u_t)_{\text{cusp}}] - \int_{\ell_{\text{cusp}}}^{\ell_{\text{in}}} \frac{\Omega d\ell}{1 - \Omega\ell} . \tag{22}$$

On the other hand, the outer edge of the torus ϖ_{out} is defined as the position at which $P = 0$ and it is obtained by integration of the hydrostatic balance equation (13). Then, for a given distribution of specific angular momentum, sequences of tori having the same ϖ_{max} but different radial extents can be constructed by varying the potential gap ΔW_{in}.

In order to investigate how the axisymmetric oscillations depend on the parameters of the discs, we have constructed sequences of models, having different radial extents and different distributions of specific angular momentum. The main properties of the various models considered are listed in Table 1. Models of class A (henceforth models A) are sequences of equilibrium tori with a constant distribution of specific angular momentum, while models B and C have a specific angular momentum increasing outwards according to Eq. (21). Unlike models A and C, which correspond to sequences of discs with different radial sizes for a given pair of values of ℓ_c and q, models B, refer to different disc sequences which not only have different radial sizes but also different values of the power-law index q for each of the constant coefficients ℓ_c; that is for each set of models from B1 to B10, we have constructed discs with values of the power-law index q varying between the minimum and maximum values listed in the fourth column of Table 1 at intervals of $\Delta q = 0.005$. The last sequence, C8, correspond to discs with a distribution of angular momentum having a power-law index $q \sim 0.4$, close to the Keplerian value $q_{kep} \equiv 0.5$. Therefore, all these models allow for an extensive investigation of the parameter space in terms of disc sizes and distributions of specific angular momentum, varying from constant to almost Keplerian.

---

[3] Note that Qian et al. (2009) considered an alternative ansatz for the distribution of the specific angular momentum.
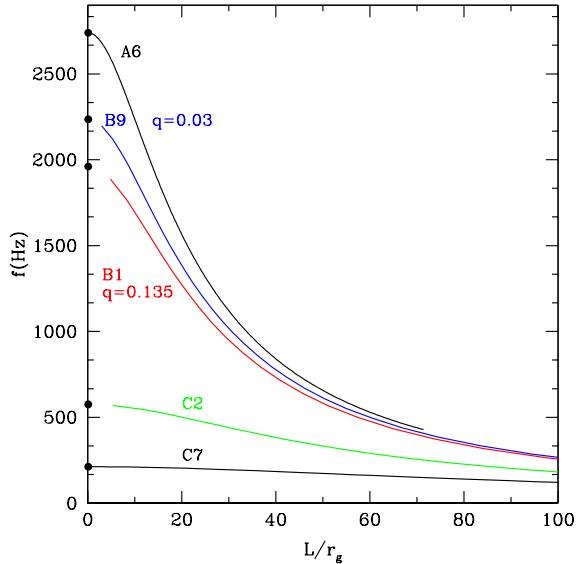
Figure 1. Eigenfrequencies for the fundamental mode of axisymmetric p modes for some representative tori with constant and nonconstant distributions of specific angular momentum. Each line corresponds to a sequence of tori having the same ϖ_{max} but different radial extents L and the solid circles correspond to the values of the Keplerian radial epicyclic frequency at ϖ_{max} in the Hartle-Thorne metric.

Figure 2. Ratio o_1/f as function of the radial size of the disc for models with a constant distribution of specific angular momentum, i.e. models A1 to A6.

5 RESULTS OF THE GLOBAL ANALYSIS

The main properties of axisymmetric oscillations of tori in a Hartle-Thorne background are analogous to those found for tori in a Schwarzschild and Kerr spacetimes (Paper I and Paper II). Overall, a fundamental mode of oscillation and a sequence of overtones are found (collectively referred to as p-mode oscillations) which depend on the position of the rest-mass density maximum, on the radial size of the disc, on the distribution of angular momentum, while they are rather independent of the equation of state (Rezzolla et al. 2003; Montero et al. 2004; Zanotti et al. 2003; Zanotti et al. 2005; Montero et al. 2007). These properties can be summarized as follows:

• The eigenfrequencies of p-mode oscillations increase as the radial size of the disc decreases.

• The fundamental-mode tends to the values of the radial epicyclic frequency at the position of the rest-mass density maximum as the radial size of the tori tends to zero.

• For any radial extent, the model with the largest fundamental-mode eigenfrequency has its rest-mass density maximum located at the position at which the epicyclic frequency has a maximum.

• The ratio between the frequency of the fundamental-mode (f) and its first overtone (o_1) for tori with constant distributions of specific angular momentum, $\ell(\varpi) = \text{const.}$, appear approximately in a 2:3 ratio. As the size of the tori tends to zero, the ratio o_1/f tends to $o_1/f \sim 1.52$.

• The ratio between the frequency of the fundamental-mode (f) and its first overtone (o_1) for tori with nonconstant distributions of specific angular momentum, $\ell(\varpi) = \ell_c \varpi^q$ can deviate significantly from $o_1/f \sim 3/2$ for very small discs. As the size of the disc increases the o_1/f ratio tends to $o_1/f \sim 1.44$.

In Figure 1, we show the eigenfrequencies (in units of Hz and scaled for a neutron star mass $M = 1.6 M_\odot$) for the fundamental
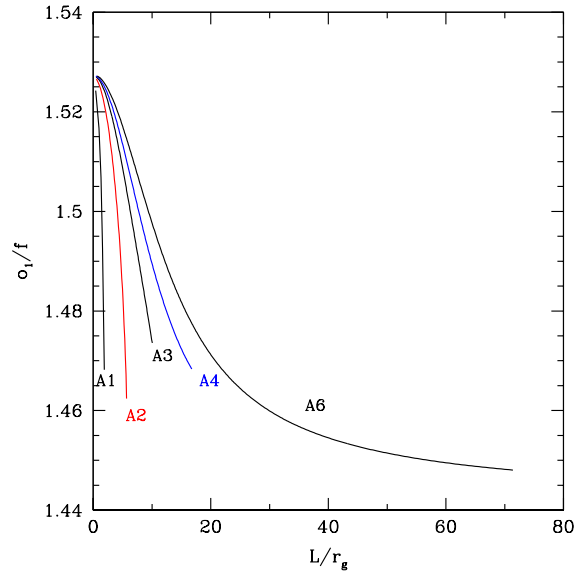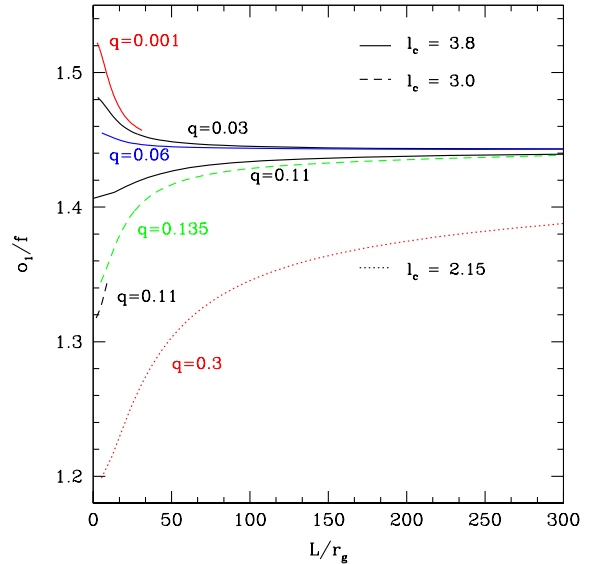

Figure 3. Ratio o_1/f as function of the radial size of the disc for some representative models with a nonconstant distribution of specific angular momentum, i.e. models B and C.

mode corresponding to some representative tori of our sample (i.e., A6, B9 with $q = 0.03$, B1 with $q = 0.135$, C2, and C7) and reported as a function of the radial size of the disc expressed in units of the gravitational radii $r_g \equiv GM/c^2$. Each line corresponds to a sequence of tori having the same ϖ_{max} but different radial extents L and the solid circles correspond to the values of the Keplerian radial epicyclic frequency at ϖ_{max} in the Hartle-Thorne metric (Abramowicz et al. 2003). As expected for modes behaving effectively as sound waves trapped in the disc, the eigenfrequencies decrease like L^{-1} as the radial extent of the torus increases. Note also

that, as was shown in Paper I and Paper II for tori orbiting around a Schwarzschild and a Kerr black hole, the eigenfrequencies of the fundamental mode tend to the values of the radial epicyclic frequency at ϖ_{max} as the radial dimension of the discs tends to zero. As their size diminishes, the role of pressure gradients inside the disc becomes negligible and the discs effectively behave as rings of particles in circular orbits, oscillating with the epicyclic frequency at the maximum rest-mass density point.

A key feature of the axisymmetric p-modes oscillations of tori around black holes is that the eigenfrequencies of the fundamental mode and the first overtone appear in an approximately 2:3 harmonic sequence, although deviations are possible, in particular for the nonconstant specific angular momentum case. This feature is also present in the case of sub-Keplerian discs in the Hartle-Thorne spacetime. In Figure 2 we show the ratio o_1/f as a function of the radial size of the disc for models with a constant distribution of specific angular momentum, i.e. models A1 to A6. As the size of the disc decreases the o_1/f ratio increases and tends to a value of ~ 1.52, independently of the constant distribution of specific angular momentum. On the other hand, the behaviour of the o_1/f ratio, as the disc size decreases, is more complex for nonconstant angular momentum disc. In Figure 3 we plot the ratio o_1/f as function of the radial size of the disc for some representative models with a nonconstant distribution of specific angular momentum. These models belong to the sequences B and C, and the values of the constant coefficient ℓ_c and of the power-law index q are also shown in Figure 3. We observe that for small discs, the o_1/f ratio decreases as the power-law index q increases for a given value of constant coefficient ℓ_c, i.e. there exists a variation of about 30% in the o_1/f ratio for small discs. In particular, o_1/f has an upper limit of ~ 1.52 (for discs with an almost constant distribution of specific angular momentum), and a lower limit of ~ 1.15 for models with a power-law index q close to the Keplerian value $q_{kep} = 0.5$. On the other hand, for large-size discs the o_1/f ratio tends to $o_1/f \approx 1.44$.

6   IMPLICATIONS FOR KHZ-QPOS IN NEUTRON STAR LOW MASS X-RAY BINARIES

Based on these properties of the axisymmetric p-modes oscillations of thick discs, Rezzolla et al. (2003) proposed a model of kHz-QPOs in BHBs that explains the observed frequencies in terms of p-modes oscillations of a small accretion thick disc orbiting close to the black hole (Schnittman & Rezzolla 2006). This model accounts very well for the M^{-1} scaling of the observed frequencies, for the observed variations in the relative strength of the peaks, that are interpreted as due to variations in the perturbations that the torus is experiencing, and for the fact that twin kHz-QPOs in the four BHBs show frequencies obeying the ratio $3 : 2$ to a high degree of accuracy. As discussed in the Introduction, on the other hand, the phenomenology of kHz-QPOs in NSBs present peculiar features that distinguish them from those detected in BHBs. In particular, the upper and lower kHz-QPOs frequencies ν_U and ν_L can vary by hundred of Hertz along straight lines $\nu_U = A\nu_L + B$, with $B \neq 0$. For convenience, we have listed in Table 2 the best fit linear parameters obtained by Belloni et al. (2005, 2007) for the Atoll sources, Z sources, Sco X-1 and Cir X-1, highlighting the linear correlation between ν_U and ν_L (errors at 1σ significance level).

Left and right panels of Figure 4 show the frequency of the upper kHz-QPO versus the frequency of the lower kHz-QPO for

Table 2. Best fit linear parameters obtained by Belloni et al.(2005,2007) for the Atoll sources, Z sources, Sco X-1 and Cir X-1.

Source	A	B
Atoll sources	0.94 ± 0.02	350 ± 15
Z sources	0.85 ± 0.01	383 ± 8
Sco X-1	0.73 ± 0.01	469 ± 7
Cir X-1	2.34 ± 0.47	104 ± 58

each class of available NSBs. We have indicated Atoll sources[4] with an asterisk, Z sources[5] with open circles, Sco X-1 with solid circles, Cir X-1 with squares and XTE J1807-294 with triangles. In addition, for all models for which we have solved the eigenvalue problem and that are listed in Table 1, we have plotted, in the relevant range of frequencies for kHz-QPOs, the first-overtone versus the fundamental mode frequencies (left panel) and the second-overtone frequency against the fundamental mode frequency (right panel). As it is shown in both panels of Figure 4, the portion of the plot covered by the observational data intersect only marginally with the values obtained from the eigenmode analysis. In particular, we show on the left panel, that there are discs (mostly B models) with fundamental mode frequency $f > 500$ Hz and a first-overtone frequency which can be in agreement with most observed ν_L and ν_U kHz-QPO frequencies for Sco X-1, and for some Z sources and Atoll sources. This range of fundamental mode frequencies ($f > 500$ Hz) indicates that the corresponding suitable models would be small in size (L smaller than $\approx 50 \mathrm{r}_g$), and would have a nonconstant distribution of specific angular momentum (B models).

On the contrary, we do not find models lying above the line with constant slope $3 : 2$, which would be needed to explain the observed twin QPOs with $\nu_L \lesssim 500$ Hz. As shown in Figure 1, the fundamental mode frequency decreases as the size of the disc increases or as the distribution of specific angular momentum approaches the Keplerian profile. The o_1/f ratio tends to $o_1/f \sim 1.44$ as the size of the disc increases or to smaller values for small discs with (see Figure 3). This reflects in the tendency, that models show, to concentrate towards the $3 : 2$ ratio line as the fundamental mode frequency tends to zero (left panel of Figure 4).

The possibility that the observed ν_L and ν_U kHz-QPO frequencies correspond to the fundamental frequency and to the second overtone of an oscillating torus, encounters similar difficulties (see right panel of Figure 4). Although the area covered by the computed p-modes oscillations match some of the observed kHz-QPO frequencies, particularly those of Z sources with ν_L in the range $150 - 500$ Hz, the observations of most of the Atoll sources, of Cir X-1 and of several Z sources remain unexplained.

Overall, the properties of axisymmetric p-mode oscillations of vertically integrated thick discs are such that, in a plot ν_U versus ν_L, the first-overtone and the fundamental mode frequency follow a straight line for which A may depart from an exact $3 : 2$ ratio by 30% (in the case of discs with a nonconstant distribution of the specific angular momentum), but for which $B \approx 0$.

---

[4] 4U 1728-34, 4U 0614+09, 4U 1705-44, KS 1731-260, 4U 1735-44, 4U 1608-52, 4U1636-53, 4U 1820-30, 4U 1915-05, XTE J2123-058.
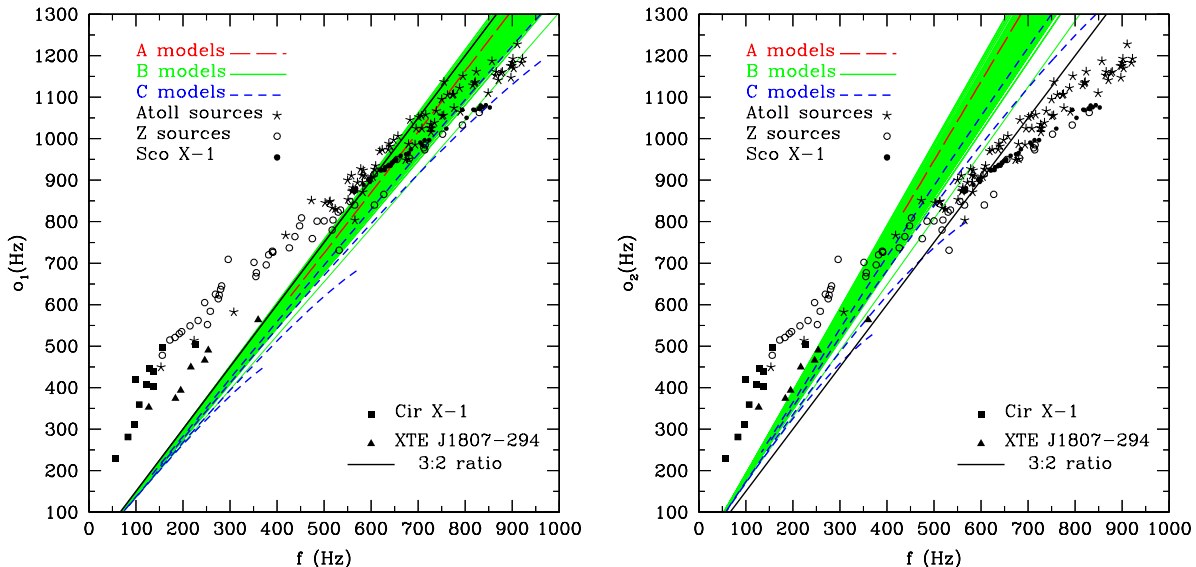[5] GX 17+2, GX 5-1, GX 340+0, Cyg X-2, CX 349-2.

Figure 4. Left panel shows a linear plot of the frequency of the upper kHz QPO versus the frequency of the lower kHz QPO with an asterisk for the Atoll sources, circles for the Z sources, solid circles for Sco X-1, squares for Cir X-1 and triangles for XTE J1807-294. We also plot, in the relevant range of frequencies for kHz QPOs, the first-overtone versus the fundamental mode frequencies for all models listed in Table 1. Right panel shows the second-overtone versus the fundamental mode frequencies instead.

7 CONCLUSIONS

We have performed a detailed analysis of the oscillation properties of a thick disc (torus) around a slowly rotating neutron star. Our approach extends previous investigations by Rezzolla et al. (2003) and Montero et al. (2004) by considering a much wider parameter space and by solving the linear perturbative eigenvalue problem in the Hartle-Thorne metric. In particular, the rotation law of the torus spans the whole range between a constant distribution of the specific angular momentum and an almost Keplerian rotation. We have computed a fundamental mode of oscillations and a sequence of overtones which can in principle be all excited depending on the perturbation acted upon the torus.

We showed there are discs (B and C models) with fundamental mode frequency $f \gtrsim 500$ Hz and a first-overtone frequency which can be in agreement with most observed ν_L and ν_U kHz-QPO frequencies for Sco X-1, and for some Z sources and Atoll sources.

However, when these results are used for explaining kHz-QPOs in neutron star low mass X-ray binaries with twin QPOs with $\nu_L \lesssim 500$ Hz, a major difficulty arises. In fact, unlike kHz-QPOs in black hole binaries, the upper and the lower kHz-QPOs in neutron star binaries obey a linear relation $\nu_U = A\nu_L + B$, with A significantly different from 1.5 (e.g. $A \approx 0.94$ for Atoll sources, $A \approx 0.85$ for Z sources and $A \approx 0.73$ for Sco X-1) and $B \neq 0$. On the contrary, the computed axisymmetric p-modes, either in the ratio o_1/f or o_2/f follow a straight line with $0.8 \lesssim A \lesssim 1.5$ and with $B \approx 0$ for o_1/f, and with $A \gtrsim 1.5$ and $B \approx 0$ for o_2/f. Therefore, unless additional physical effects are taken into account, such as the interaction of the accreting thick disc with the surface of the neutron star, the presence of a magnetic field (Balbus & Hawley 1991), or non-axisymmetric instabilities (Papaloizou & Pringle 1984; Kiuchi et al. 2011), axisymmetric p-modes oscillations of a thick disc around a neutron star do not provide an explanation for the observed twin QPOs in neutron star X-ray binaries with $\nu_L \lesssim 500$ Hz.

REFERENCES

Abramowicz M., Kluzniak W., Bursa M., Horák J., Rebusco P., Török G., 2007, in Revista Mexicana de Astronomia y Astrofisica, vol. 27 Vol. 27 of Revista Mexicana de Astronomia y Astrofisica Conference Series, The Twin Peak QPOs in Neutron Star and Black Hole Sources: What is explained, and What is not. pp 8–17

Abramowicz M. A., G.J.E. A., Kluźniak W., V. T. A., 2003

Abramowicz M. A., Karas V., Kluzniak W., Lee W. H., Rebusco P., 2003, Pub. Astron. Soc. Japan, 55, 467

Arras P., Blaes O., Turner N. J., 2006, Astrophysical Journal Letter, 645, L65

Balbus S. A., Hawley J. F., 1991, Astrophys. J, 376, 214

Belloni T., Méndez M., Homan J., 2005, Astron. Astrophys., 437, 209

Belloni T., Méndez M., Homan J., 2007, Mon. Not. R. Astron. Soc., 376, 1133

Blaes O. M., Arras P., Fragile P. C., 2006, Mon. Not. R. Astron. Soc., 369, 1235

Boutelier M., Barret D., Lin Y., Török G., 2010, Mon. Not. R. Astron. Soc., 401, 1290

Hartle J. B., Thorne K. S., 1968, Astrophys. J., 153

Kiuchi K., Shibata M., Montero P. J., Font J. A., 2011, Phys. Rev. Lett., 106, 251102

Kozlowski M., Jaroszynski M., Abramowicz M. A., 1978, Astron. and Astrophys., 63, 209

Lamb F. K., Miller M. C., 2003, ArXiv Astrophysics e-prints

Lewin W. H. G., van der Klis M., 2006, Compact stellar X-ray sources

Miller M., 2010, New Astronomy Review, 54, 128

Miller M. C., Lamb F. K., Psaltis D., 1998, Astrophysical Journal, 508, 791

Montero P. J., Font J. A., Shibata M., 2008, Phys. Rev. D, 78, 064037

Montero P. J., Font J. A., Shibata M., 2010, Phys. Rev. Lett., 104, 191101

Montero P. J., Rezzolla L., Yoshida S., 2004, Mon. Not. R. Astron. Soc., 354, 1040

Montero P. J., Zanotti O., Font J. A., Rezzolla L., 2007, Mon. Not. R. Astron. Soc., 378, 1101

Muno M. P., Chakrabarty D., Galloway D. K., Savov P., 2001, Astrophys. J. Lett., 553, L157

Novikov I. D., Thorne K. S., 1973, in Black Holes (Les Astres Occlus) Astrophysics of black holes.. pp 343–450

Papaloizou J. C. B., Pringle J. E., 1984, Mon. Not. R. Astron. Soc., 208, 721

Qian L., Abramowicz M. A., Fragile P. C., Horák J., Machida M., Straub O., 2009, Astron. and Astrophys., 498, 471

Remillard R. A., McClintock J. E., 2006, Ann. Rev. Astron. Astroph., 44, 49

Rezzolla L., Ahmedov B. J., Miller J. C., 2001, Mon. Not. R. Astron. Soc., 322, 723

Rezzolla L., Yoshida S., Maccarone T. J., Zanotti O., 2003, Mon. Not. R. Astron. Soc., 344, L37

Rezzolla L., Yoshida S., Zanotti O., 2003, Mon. Not. R. Astron. Soc., 344, 978

Sanna A., Méndez M., Altamirano D., Homan J., Casella P., Belloni T., Lin D., van der Klis M., Wijnands R., 2010, Mon. Not. R. Astron. Soc., 408, 622

Schnittman J. D., Rezzolla L., 2006, Astrophysical Journal, 637, L113

Stella L., Vietri M., 1999, Phys. Rev. L., 82, 17

Török G., Abramowicz M., Kluźniak W., Stuchlík Z., 2006, in J.-M. Alimi & A. Füzfa ed., Albert Einstein Century International Conference Vol. 861 of American Institute of Physics Conference Series, A non-linear resonance model for the black hole and neutron star QPOs: theory supported by observations. pp 786–793

Török G., Abramowicz M. A., Bakala P., Bursa M., Horák J., Kluzniak W., Rebusco P., Stuchlik Z., 2008, Acta Astronomica, 58, 15

Török G., Abramowicz M. A., Kluźniak W., Stuchlík Z., 2005, Astron. Astrophys., 436, 1

van der Klis M., 2005, Astronomische Nachrichten, 326, 798

van Straaten S., van der Klis M., Mndez M., 2003, Astrophys. J., 596, 1155

Wilson J. R., 1972, Astrophys. J., 173, 431

Zanotti O., Font J. A., Rezzolla L., Montero P. J., 2005, Mon. Not. R. Astron. Soc., 356, 1371

Zanotti O., Rezzolla L., Font J. A., 2003, Mon. Not. Roy. Soc., 341, 832

Zhang C. M., 2004, Astron. Astrophys., 423, 401